Available online at www.sciencedirect.com

SciVerse ScienceDirect

Ceramics International 39 (2013) 2665–2674

CERAMICS INTERNATIONAL

www.elsevier.com/locate/ceramint

Yttria stabilized zirconia formed by micro ceramic injection molding: Rheological properties and debinding effects on the sintered part

Farhana Mohd Foudzi[a], Norhamidi Muhamad[a], Abu Bakar Sulong[a,*], Hafizawati Zakaria[a,b]

[a]*Department of Mechanical and Material Engineering, Faculty of Engineering and Built Environment, Universiti Kebangsaan Malaysia, 43600 UKM Bangi, Selangor, Malaysia*

[b]*Department of Mechanical Engineering, School of Mechanical and Manufacturing Engineering, Universiti Malaysia Perlis, Ulu Pauh, 02600 Arau, Perlis, Malaysia*

Received 20 July 2012; received in revised form 10 September 2012; accepted 10 September 2012
Available online 18 September 2012

Abstract

Micro Ceramic Injection Molding (μCIM) is a near net-shape process to produce smaller and intricate parts at a competitive cost. The application of nano-sized ceramic powder in μCIM has the advantages of fine grain size growth and good surface finish. However, the nano size effect causes agglomeration and low powder loadings, which result in defects during the μCIM process and in the sintered components. This study extensively investigated the debinding and sintering of yttria-stabilized zirconia (YSZ), as well as its rheological properties, using polypropylene (PP) as the primary binder and palm stearin as the secondary binder. 50 nm Yttria stabilized zirconia (YSZ) powders were mixed with palm stearin and PP at a powder loading of 37–43 vol%. The results of rheological studies showed that the feedstock had a dilatant flow characteristic and a viscosity of around 10–40 Pa s. Feedstock with 38 vol% powder loading had the lowest activation energy of 9.48 kJ/mol. The green part of the injected feedstock had flexural strength ranging from 13 to16 MPa, within which the feedstock with 43 vol% powder loading had the highest green density. Solvent debinding was carried out at three temperatures (50, 60, and 70 °C) using heptane. A large porous region was clearly identified at 70 °C compared with 50 °C. A debinding split furnace with argon gas was used to remove PP at 450 °C for 4 h. The debound samples did not shrink when 94%–98% of the binder system was removed. All debound samples sintered at 1350 °C and 41 vol% had the highest mechanical properties with hardness of 900 HV and a flexural strength of 400 MPa.

Keywords: C. Mechanical properties; Micro ceramic injection molding (μCIM); Nano sized zirconia; Rheological properties

1. Introduction

μCIM is used for the low-cost mass production of small parts with complex features in various industries [1]. High quality, near-net-shaped products can be generated by a minimum finishing procedure that involves four main processes: mixing, injecting, debinding and sintering [2]. Zirconia has three forms: pure, partially and fully stabilized. The addition of stabilizers such as yttria (Y_2O_3), ceria (CeO_2), and calcia (CaO) enables zirconia to form a cubic phase at room temperature [3]. Raw material characteristics are very important in obtaining both physical and mechanical properties which help in designing the parameters involved in each of the main four processes. The rheology test is important in determining the flow behavior that influences the successful of injection process [4]. Instability, powder binder separation and poor rheological behavior can be detected during this test.

Few researches have reported the great advantages of using a palm stearin-based binder system, including its low cost, wide availability and good properties [5,6,8–10]. Palm stearin is best known for its ability to provide a capillary route for the removal of remaining binder in the later stage of debinding prior to sintering [6]. Debinding is a crucial process for removing the binder system to achieve a high density without the influence of any defects produced by the binder in the early stage [7]. Many researchers have

*Corresponding author. Tel.: +603 89216678; fax: +603 89259659.
E-mail address: abubakar@eng.ukm.my (A. Bakar Sulong).

0272-8842/$ - see front matter © 2012 Elsevier Ltd and Techna Group S.r.l. All rights reserved.
http://dx.doi.org/10.1016/j.ceramint.2012.09.033

used 60 °C to remove palm stearin from the green part for 4–5 h in a heptane solution [8,9]. Palm stearin ratio of 70 wt% results in better mechanical properties than 60 wt% [10]. Polypropylene (PP), a thermoplastic, is well known to maintain the component shape after injecting and debinding [11]. The remaining PP or PE binders are removed by thermal debinding at a heating rate of 1 °C/min until 450 °C [8]. Sintering is the final stage in the metal injection molding (MIM) process and the properties of the products are evaluated by several mechanical tests [7]. The reported optimum sintering temperature for 3 mol%YSZ is 1350 °C, which produces fine grains with a high hardness of 1200 HV and 10% to 23% shrinkage. A 15% shrinkage in MIM products is common. However, 25% was reported for micro feature parts due to very fine particles resulting in difficulty obtaining the final density near the theoretical value [12]. This study aimed to determine the feasibility of palm stearin as a secondary binder of feedstock during injection molding. The effects of debinding temperature on the physical and mechanical properties of the sintered part were analyzed.

2. Methodology

The 3 mol% YSZ powder purchased from Nabond Technologies (China) had an average particle size of 50 nm, as reported by the manufacturer. Its pycnometer density of 6.43 g/cm^3 was measured using a Micromeritics Accu Pyc, model 1330. Palm stearin was supplied by Intercontinental Fats Sdn. Bhd. PP was purchased from Titan Chemicals Sdn Bhd. Scanning electron microscopy (SEM) was used to determine the physical geometries of 3 mol%YSZ powder and palm stearin, as shown in Fig. 1. Fig. 1(a) shows the near circular particle shape of 3 mol% YSZ powder which is ideal for MIM [13]. The flake particle shape of palm stearin is shown in Fig. 1(b).

The elemental contents of 3 mol% YSZ powder and palm stearin were determined by energy dispersive X-ray spectroscopy (EDX) associated with field emission SEM (Zeiss Supra 55VP). The elemental contents of 3 mol% YSZ were found to be 54.55 wt% zirconia, 10.49 wt% carbon, 31.91 wt% oxygen, 1.35 wt% yttria, and 1.70 wt% hafnium. Palm stearin contained 90 wt% carbon and 10 wt% oxygen. The elemental content determination was important in determining the influence of the μCIM process on elements of the sintered component. A roller blade type internal mixer (Thermo-Haake) was used to determine the critical powder loading of 3 mol% YSZ [14]. Differential scanning calorimetry (DSC) analysis was carried out to determine the binder melting point used in the feed stock using a Mettler Toledo DSC 822E. Each binder degradation temperature was obtained by thermogravimetric analysis (TGA) using Rigaku Thermaflex at a heating rate of 10 °C/min. Both DSC and TGA results were used as references for temperature determination of the solvent and thermal debinding. A roller blade-type Brabender mixer (GmbH & Co., KG) was used in all powder loading mixing processes. A mixing temperature of 180 °C was maintained with a constant speed of 20 rpm for 1 h until a dough-like mixture was achieved. The pellet-form feedstock was produced by crushing using a heavy duty crusher machine. The rheological properties were measured using a Shimadzu CFT-500D at various temperatures (180, 190 and 200 °C). The injection process was conducted using a 10 ccm plunger type DSM Xplore Injection Molding Machine. The involved injection parameters such as mold and melt temperatures, pressure and time were manipulated for each powder loading to obtain the best results with no defects such as shot, cracking and flashing. Table 1 shows the injection parameter values.

The green density was measured by an electronic balance (Sartorius, model BSA224S-CW) with four decimal points using distilled water as the medium. The flexural properties of the green parts with powder loadings of 37–43 vol% were examined using a Universal Testing Machine (3 t, model 5567). The debinding stage was divided into solvent and thermal debinding. Heptane was used to remove palm stearin at three different temperatures (50, 60 and 70 °C) for 6 h using a Furnace Dryer WTB Binder, model 950204. The remaining binder, (PP), was removed using a Debinding Split Furnace, model RS800/200/200 at 450 °C for 4 h. The weighing process and surface morphological evaluation of the debound part were performed after solvent and thermal debinding. All debound parts were sintered at

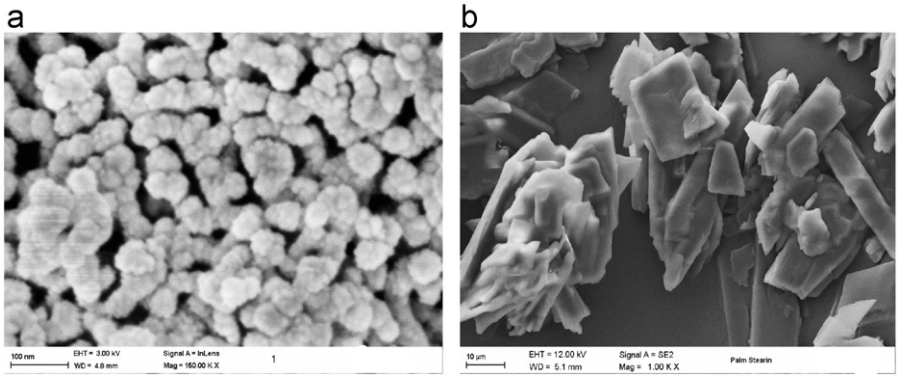

Fig. 1. SEM images of (a) 3 mol% YSZ and (b) Palm stearin.

Table 1
Injection parameters used for each powder loadings.

Powder loading (vol%)	Melt temperature (°C)	Injection temperature (°C)	Pressure (bar)	Injection time (s)
37	60	180	4:5:5	6:8:6
38	65	190	5:6:6	6:8:6
39	65	190	5:6:6	6:8:6
40	65	190	5:6:6	6:8:6
41	65	190	5:6:6	6:8:6
42	70	190	6:7:7	7:8:7
43	70	190	6:7:7	7:8:7

1350 °C for 6 min. The mechanical properties were analyzed by tensile and flexural tests using a Universal Testing Machine (3 t, model 5567). The hardness of the sintered part was measured using Metallic Vickers Tester, model MITAKA HVS10, with a dwell load of 1 kg. The morphological investigation was conducted on the surface and fractured surface of the sintered part after tensile test using FESEM, model Zeiss Supra 55VP. The densities of the sintered parts were determined using a mass balance Sartorius model BSA224S-CW based on the Achimedes method. The carbon and sulfur contents were measured using a Carbon/Sulfur Determinator, model LECO CS-244 and the oxygen content was determined using an ONH Gas Analyzer. The sintered part of nano-zirconia with palm stearin based binder system that had the best properties was chosen with the most suitable powder loading, injection parameters and debinding temperature. All characterizations of the sintered part were based on MPIF 2006 (standard test methods for metal powders and powder metallurgy products) [15].

3. Results and discussion

3.1. Material characterization

Fig. 2(a and b) shows the DSC curve for palm stearin and PP, respectively. Palm stearin and PP started to melt at ~70 °C and ~160 °C, respectively. The mixing process was carried out based on the highest recorded melting point but lower than the degradation temperature to melt and ease the binder system completely for homogeneous mixing [13]. PP has the highest melting point, thus the mixing process was conducted at 180 °C, which was slightly higher from the recorded value (Fig. 2(b)) [14].

The degradation temperatures of palm stearin and PP were obtained by TGA analysis, and the results are shown in Fig. 3. Fig. 3 shows that palm stearin started to degrade at 200 °C and ended beyond 500 °C, whereas PP began to degrade at 173.68 °C and ended at 411 °C. The measured critical powder loading (CPVP) was 45.26 vol% with 22 ml of oleic acid added [14]. Thus, the selected powder loading range of 37–43 vol%, which was 3%–5% lower than the measured CPVP. However, this range was still lower than the ceramic range of 50–55 vol% as reported by German and Bose [16]. The nano-size ceramic had a higher surface area, thus a higher binder fraction was required to cover each powder particle [17]. Based on previous research, the lowest and highest loadings were 26 vol% and 60 vol%, respectively [7,18,19]. The most critical stages are the debinding and sintering processes where large shrinkage percentage affects the strength and toughness of the sintered product [20].

3.2. Rheological properties

Fig. 4 shows variations in all powder loading viscosities against shear rates, indicating their rheological properties. The dilatant flow associated with the flowability index, n was more than 1 [16]. Thus, all powder loading n values ranged from 1.002–1.006, as shown in Fig. 4. All powder loadings showed dilatant flow characteristics in terms of increased viscosity with increased shear rates based on results in Fig. 4, which differed from the preferred type of the feedstock with pseudoplastic flow characteristics in MIM (Metal Injection Molding) [16]. However, the measured viscosity and shear rate range of 10–40 Pa s and 1000–5000 s^{-1} were under an injectable range of the feedstock for MIM process (viscosity below 1000 Pa s and shear rate ranging from 10^2–10^5 s^{-1}). The feedstock viscosity increased with increased powder loading because more particles existed, resulting in higher fractions when extruding the molten feedstock through a 1 mm die of capillary rheometer. The feedstock range of 41–43 vol% had the highest measured viscosity.

Sensitivity of each powder loading was determined by the Arrhenius equation measured by the activation energy, E (kJ/mol) [13,16]. In the MIM process, the feedstock with the lowest E value is preferable since fewer defects will be produced due to low sensitivity towards pressure and temperature. This characteristic is very important during the injection process, where defects such as cracks and deterioration can be minimized [21]. Table 2 shows the activation energy, E values. The 38 vol% and 43 vol% samples showed the lowest E value of 9.482592 kJ/mol and the highest E of 37.91 kJ/mol, respectively. The dilatant flow was associated with the powder-binder separation but the injection process was conducted to determine the injectability.

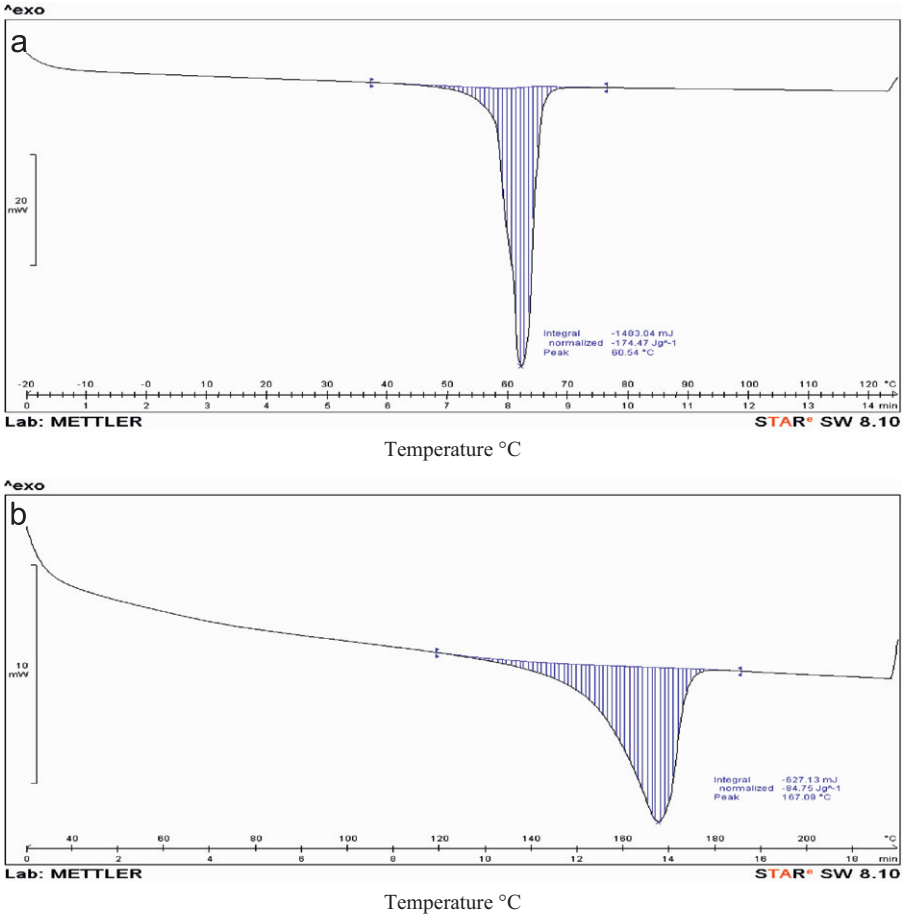

Fig. 2. Different Scanning Calorimetry curve of (a) Palm stearin and (b) PP.

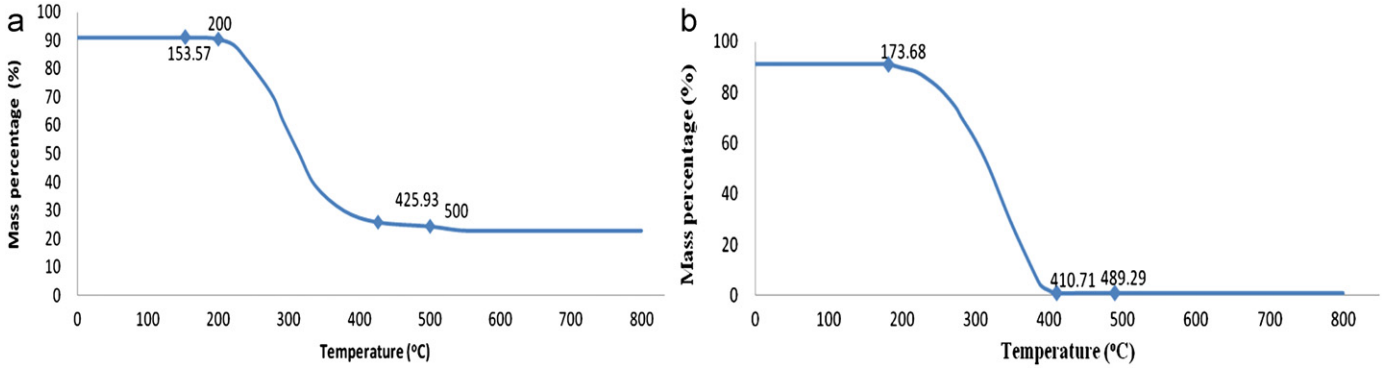

Fig. 3. Thermogravimetric curve of (a) Palm stearin and (b) PP.

3.3. Injection process

The injection process was successfully conducted on all powder loadings from 37 to 43 vol%. Short shot and flashing types of defects were observed with lower or higher applied pressure. The most suitable injection parameters were 65 °C, 190 °C and 5:6:6 ratio and 8 min for melt temperature, injection temperature, injection pressure, and holding time, respectively. The most dominant parameter was pressure, where defects were easily produced when the applied pressure was changed by 1 bar.

3.4. Debinding process

Fig. 5 shows the surface SEM images of the solvent debound specimens at 50, 60, and 70 °C. A massive void region was observed with increased temperature from 50 to 70 °C, shown in Fig. 5(a–c) because of the palm stearin

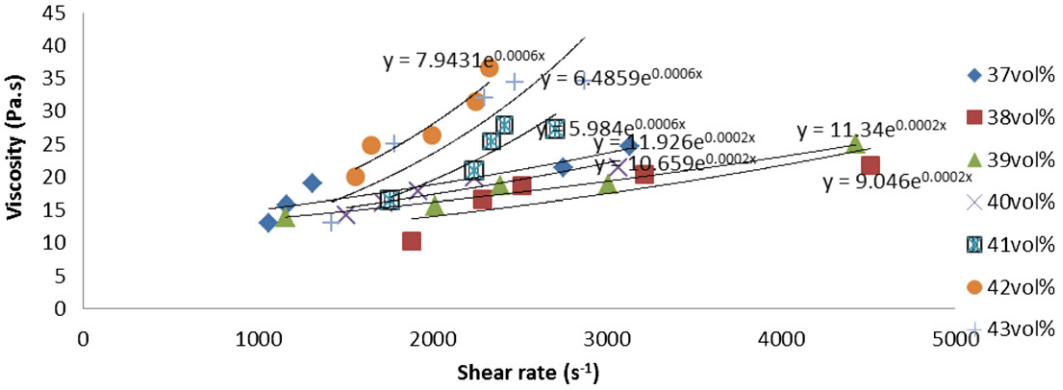

Fig. 4. Variation of viscosity againt shear rates for all powder loadings at 180 °C.

Table 2
Activation energy for each powder loading (vol%).

Powder loading (vol%)	Gradient (E/R)	Activation energy, E (kJ/mol)
37	1.68	13.97
38	1.14	9.48
39	3.49	29.02
40	3.44	28.60
41	3.97	33.01
42	4.01	33.34
43	4.56	37.91

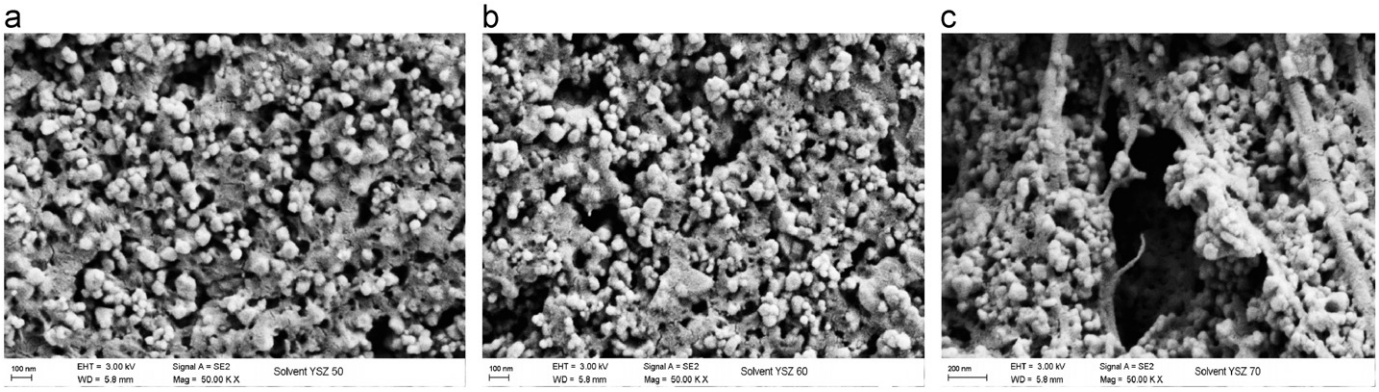

Fig. 5. Solvent debound specimen for (a) 50, (b) 60, and (c)70 °C.

melting range of 50–70 °C. The highest rate was at 70 °C. Thus massive voids were formed after the removal of palm stearin at a faster heating rate than those at 50 and 60 °C. A slight void difference between the morphologies at 50 and 60 °C was observed; more voids were present in Fig. 5(b) than in Fig. 5(a). Fig. 6 shows the surface SEM images of the thermal debound specimens after solvent debinding at 50, 60, and 70 °C. Fig. 6 shows the removal of PP with the remaining 3 mol%YSZ particles (Fig. 6(a–c)). The percentage of the removed binder system had similar range for all samples after solvent debinding. Thus, the completely debound sample at 70 °C still had the most abundant voids caused by solvent debinding. The removal of the binder system ranged from 83% to 92% after solvent debinding; the highest removal rate after debinding was at 70 °C. Palm stearin cannot be completely eliminated because its function was to provide capillary paths and holes for the remaining binder to be removed in the next debinding stage [8]. About 94%–98% of PP was removed after thermal debinding at 450 °C for 4 h with the aid of argon gas. All debound samples after thermal debinding had the same amount of remaining binder, because only one temperature was used. The remaining binder system of 2%–6% was used again to sustain its shape prior to sintering.

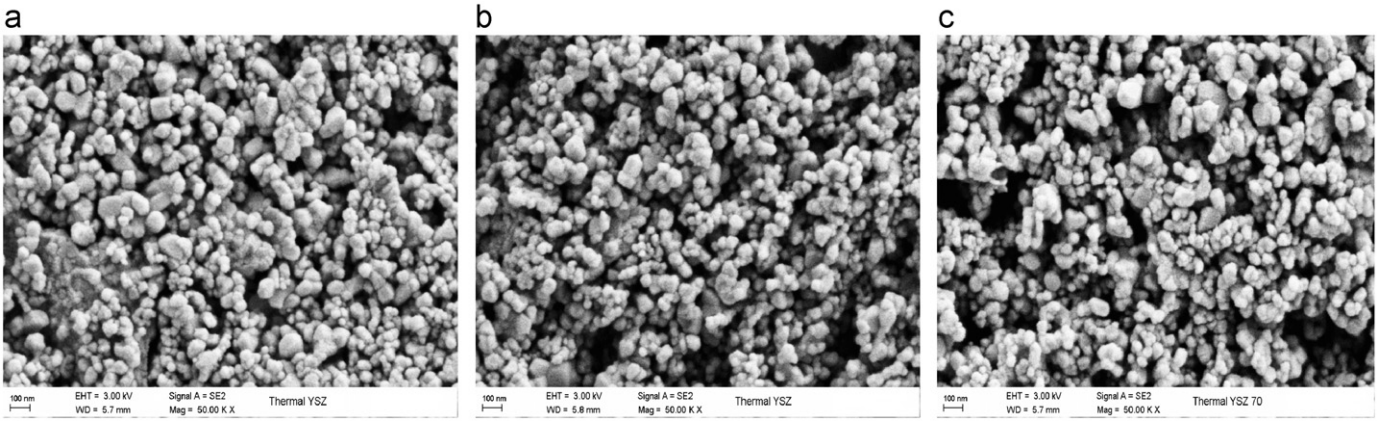

Fig. 6. Thermal debound specimen after solvent debinding at (a) 50 (b) 60 and (c) 70 °C.

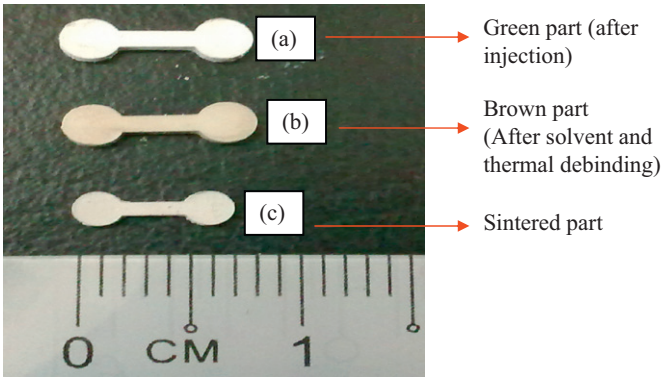

Fig. 7. Physical changes of (a) green part, (b) brown part and (c) sintered part.

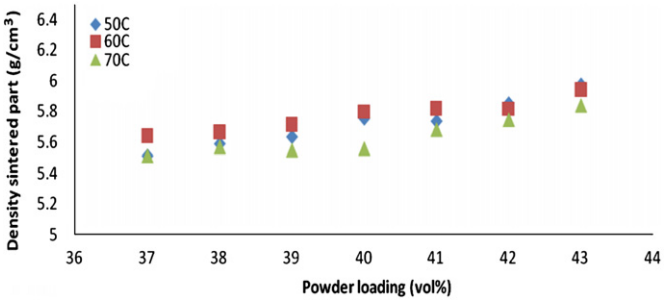

Fig. 8. Sintered density for every powder loading at all debinding temperatures.

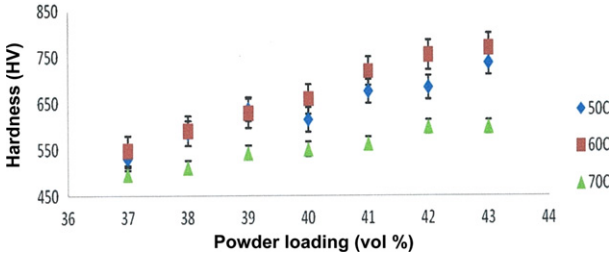

Fig. 9. Hardness of sintered parts of various powder loadings at solvent debinding at different temperatures.

3.5. Sintering process

The sintering process was conducted according to the optimum sintering cycle obtained from previous research [7]. The green and brown parts had similar dimensions as shown in Fig. 7, except for the fragile debound part where good handling was required. A significant change in the sintered part dimension was observed, i.e., its length and thickness shrunk.

3.5.1. Physical properties

The final density and shrinkage were measured after completing the sintering process. The sintered density of each powder loading (37–43 vol%) was measured to four decimal points. Fig. 8 shows the distribution data of each powder loading at different debinding temperatures. The debound part at 60 °C had the highest sintered density followed by 50 and 70 °C. Slight differences were observed in the final density of the debound parts at 50 and 60 °C, 97.9% close to the theoritical value. Voids correlated to the density properties; the density decreased with increased number of voids. The debound sample at 70 °C was observed to have the widest void region compared with those at 50 and 60 °C, as shown in Fig. 6. The sintered density values gradually increased with powder loading. However, voids were present in some samples and the readings roughly increased from 37 to 43 vol%. The sintered part underwent shrinkage ranging from 17% to 21%, which was 10%–23%% lower than the ones reported by Yu et al. using nano zirconia for micro sized products [22].

3.5.2. Mechanical properties

Fig. 9 shows the hardness of the sintered parts with increased powder loadings at different debinding temperatures. Fig. 9 indicates that 43 vol% powder loading had the highest hardness of 760 HV, whereas 37 vol% had the lowest hardness of 470 HV. These values were far from the

3 mol% YSZ theoretical hardness value of 1100 HV due to the incomplete diffused sintered parts during the sintering process as observed in the microstructure [16]. Among the three debinding temperatures, the sintered sample debound at 60 °C had the highest hardness value following those at 50 and 70 °C, with values of 760, 680 and 570 HV, respectively. The sintered parts with powder loading 37–43 vol%, debound at three temperatures, were subjected to tensile tests.

Table 3 shows tensile strength of sintered parts of various powder loadings at solvent debinding. The highest tensile test value was 39.9 MPa at 41 vol% debound at 60 °C. Similar phenomena were observed in the flexure strength test, where the highest flexure strength was measured with the same powder loading and debinding temperature. The sintered part debound at 60 °C had the highest tensile strength followed by 50 and 70 °C, within which the void regions played a role in determining the mechanical properties. The obtained value was low from 21 to 40 MPa, because of the high carbon content that weakened the ductility properties.

3.5.3. Morphology of sintered part

Morphological studies were conducted on the surface and fracture surface of the sintered part after the tensile tests. Fig. 10 shows the surface morphology of both 38 and 41 vol% debound samples at 60 °C. The grains overlapped with one another and some of the particles did not undergo the necking process because of the nearly spherical shape, similar to 3 mol% YSZ particles (Fig. 1(a)). Some of the grains grew where their grain boundaries neatly attached onto each other with size up to 250 nm. The grains were not fully diffused because nano zirconia powder can grow 10–20 times their original size [23–25]. The surface of the 41 vol% sintered part had fewer voids than the 38 vol%, which resulted in better mechanical properties. The grain boundary can withstand any external force that is applied on that particular part. With increased grain growth, the grain boundaries formed between each grain increased, thereby strengthening the bond between grains and the resistance to any external force. The 38 vol% sintered part was clearly observed to break easily compared with the 41 vol% sintered part because of weak grain-to-grain formation with many void regions (Fig. 10).

Morphological studies were carried out on the fracture surface after the tensile test for 38 and 41 vol% debound samples at 60 °C as shown in Fig. 11.Almost all 3 mol% YSZ particles were fully diffused because the majority of the particles had original, near spherical shape. More voids were observed at 38 than at 41 vol% because less powder

Table 3
Tensile strength of sintered part of various powder loading at solvent debinding temperatures of 50, 60, and 70 °C.

Powder loading (vol%)	Tensile strength (MPa) at different debinding temperatures		
	50 °C	60 °C	70 °C
37	25.41	24.64	16.61
38	25.91	28.53	18.70
39	28.21	31.11	21.36
40	21.83	33.38	19.70
41	32.33	39.90	18.66
42	26.02	38.10	21.46
43	33.91	27.12	28.17

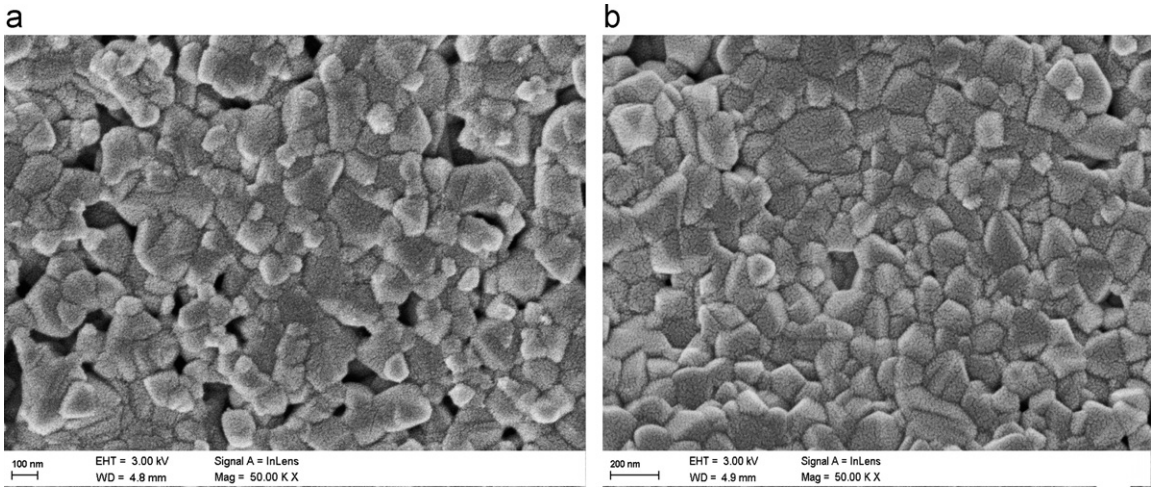

Fig. 10. Morphology of sintered specimen's surface at (a) 38 and (b) 41 vol%.

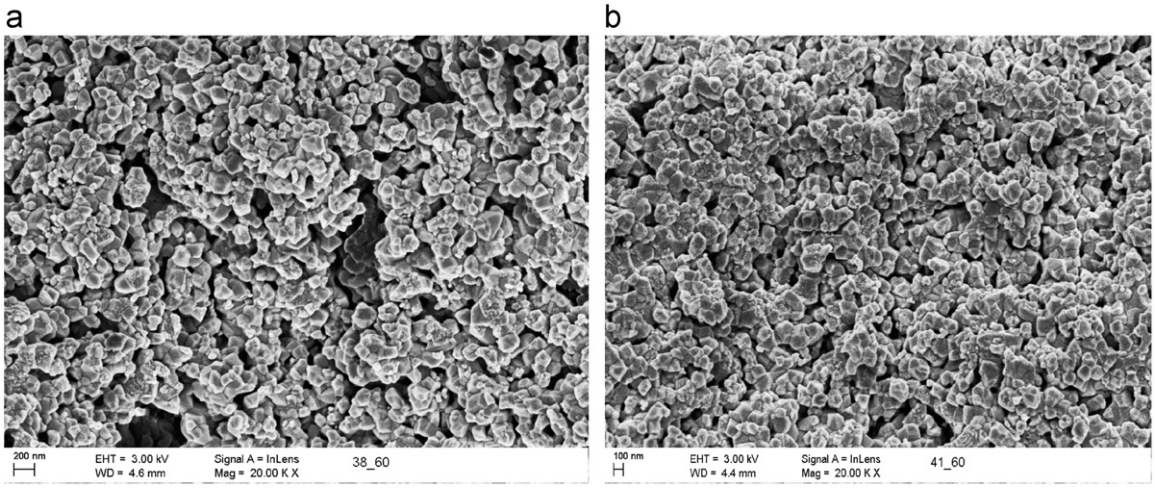

Fig. 11. Fracture surface of tensile strength (a) 38 and (b) 41 vol%, both debound at 60 °C.

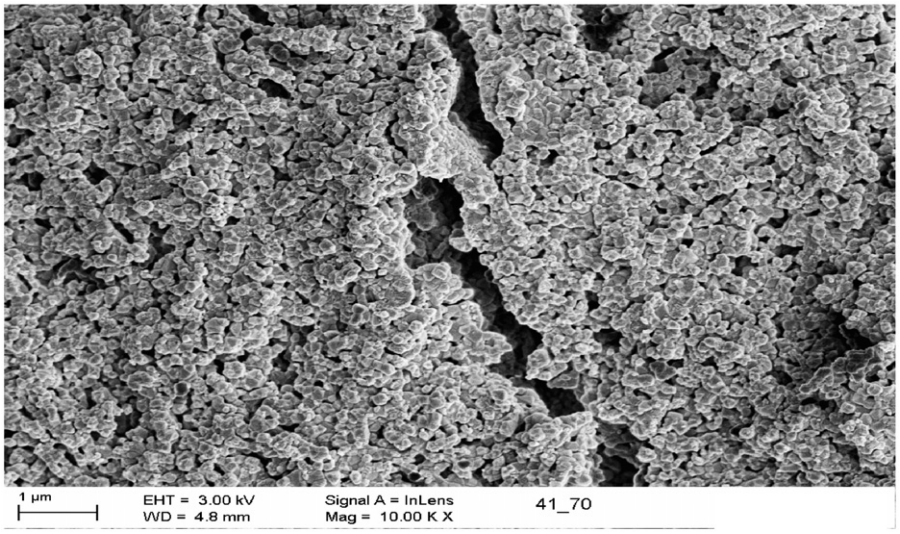

Fig. 12. Internal cracks for sintered part debound at 70 °C.

was present after removing the binder system. The fracture surface at 41 vol% was packed with 3 mol% more YSZ particles than that at 38 vol%. Thus the former had stronger and better mechanical properties (Fig. 11 (b)). The sintered surface of debound parts at 70 °C had many internal cracks that resulted in massive and abundant voids after the debinding process, as shown in Fig. 12.

The internal cracks and void regions gave low physical and mechanical test readings. The debound parts at 50 °C gave a slightly lower value than that at 60 °C due to a small difference in the void region. However, 60 °C gave the highest final density among all. A debinding temperature of 70 °C was not suitable to be applied in future works because of its weak performance during mechanical testing which resulted in internal cracks and massive void regions. The sintered part of 41 vol% debound at 60 °C gave the highest flexural strength, hardness and tensile test value, although, 38 vol% had the lowest sensitivity toward temperature and pressure in the rheological analysis. Thus, the best and most suitable debinding temperature of CIM with a palm stearin based binder system was 60 °C based on all tests, which gave better performance and properties.

3.5.4. Carbon, sulfur and oxygen contents of the sintered part

Carbon, sulfur, and oxygen contents were measured on two powder loadings (38 and 41 vol%) based on the best rheological behavior and mechanical properties; 38 vol% had the lowest E value whereas 41 vol% had the highest mechanical (hardness and flexural strength) properties. Table 4 shows the results of tests carried out at 60 °C for both 38 vol% and 41 vol%.The measured value at 60 °C was chosen based of the highest sintered density among the three debinding temperatures. For both carbon and sulfur content testing, 38 vol% showed a higher reading

Table 4
Carbon, sulfur and oxygen contents for 38 and 41 vol% debound at 60 °C.

Testing	Powder loading (vol%)	
	38	41
Carbon content	0.306	0.251
Sulfur content	0.056	0.055
Oxygen content	1.080	4.270

compared with 41 vol%. The average carbon content of sintered stainless steel (SS316L) was 0.05 wt%. However, the obtained value of 0.306 wt% in Table 3 was very high [23]. The carbon and sulfur contents for 38 vol% were higher than those for 41 vol% because of the larger binder fraction (62 vol%). With this value, a higher amount of binder than 41 vol% was present. More carbon and oxygen were present because palm stearin and PP contained substantial amounts of carbon and oxygen at a ratio of 90:10 based on the EDX test at 38 vol%. Sulfur was not detected in either powder or binder. Sulfur may contaminate or diffuse the samples throughout the processes that ended with sintering. By contrast 41 vol% had a higher oxygen content than 38 vol% in the oxygen content test. The amount of oxygen present in the powder was 31.91 wt% from EDX testing of 3 mol%YSZ powder. Thus a higher powder fraction gave a higher total oxygen content for 41 vol%. At lower powder fraction, 38 vol% had less total amount of oxygen because only 10 wt% of oxygen was present in palm stearin. All sintered parts were not fully diffused in the morphology studies; the grains overlapped with one another and some of the particles had only started to undergo necking. Thus, high oxygen content was measured for both 38 and 41 vol% because of incomplete diffusion and the high oxygen content in 3 mol%YSZ. High carbon and oxygen values helped increase the hardness properties of the parts but weakened their ductility [22].

4. Conclusion

The debinding process was successfully conducted on all powder loadings from 37 to 43 vol% at three temperatures (50, 60 and 70 °C). Abundant void regions were clearly observed at the surface part debound at 70 °C with less voids at 50 and 60 °C. The percentage of the binder system successfully removed was 92%–98% with 2%–8% still present in the parts prior to sintering. Sintering was carried out at 1350 °C with 17%–21% shrinkage. The sintered parts debound at 60 °C gave the highest final density 97.9% near the theoretical value. The powder loading of 41 vol% debound at 60 °C gave the best mechanical properties during the mechanical strength and hardness tests with values of 407 MPa and 876 HV, respectively. Morphological studies showed that all parts incompletely diffused, and some of the particles retained the grain's near-spherical shape. Internal cracks were observed on the fractured surface of the sintered part debound at 70 °C because of abundant voids after solvent debinding. The powder loading of 38 vol% had higher carbon and sulfur contents compared with 41 vol% with both debound at 60 °C. A larger fraction of the binder system gave a higher total carbon amount of 90 wt% originating from palm stearin. A higher oxygen content was measured for the 41 vol% sintered part than the 38 vol% sintered part because 3 mol% YSZ had a high oxygen content of 31.91 wt%. The debinding temperature of 60 °C was the most suitable for CIM with the palm stearin based binder system that gave less void regions, highest final density, and best mechanical properties.

Acknowledgment

The authors thank Universiti Kebangsaan Malaysia (project code UKM-AP-NBT-11-2009) for sponsoring this research, and also the Malaysia Ministry of Higher Education for a partial sponsor fellowship through the Bajet Mini program.

References

[1] V. Piotter, T. Mueller, K. Plewa, A. Ruh, H.-J. Ritzhaupt-Kleissl, J. Hausselt., Metal and ceramic micro parts produced by powder injection molding (Micro PIM), PIM Workshop (2009) May.
[2] Z.Y. Liu, N.H. Loh, S.B. Tor, K.A. Khor, Characteristic of powder injection molding feedstock, Materials Characterization 49 (2003) 313–320.
[3] W.D. Callister Jr., Fundamentals of Materials Science and Engineering, An Integrated Approach, 2nd Edition, John Wiley & Sons, Inc., 2005.
[4] B.O. Rhee, Y.C. Jung, J.H. Lee., The rheological characterization of PIM feedstocks at low shear rates, Powder Injection Molding Technologies 23 (1998) 79–91.
[5] A. Iftikhar, Significance of palm oil and palm stearin as fatty raw materials for soap, PORIM Occasional Paper, No. 13, PORIM Publication, Selangor, Malaysia, 1984.
[6] F. Ismail, M.A. Omar, I. Subuki, N. Abdullah, E.A.G.E. Ali, N. Hassan, Characterization of the feedstock for metal injection molding using biopolymer binder, Regional Conference on Engineering Mathematics, Mechanics, Manufacturing and Architecture (EM^3ARC) (2007) 85–92.
[7] P.C. Yu, Q.F. Li, J.Y.H. Fuh, T. Li, P.W. Ho, Micro injection molding of micro gear using nano-sized zirconia powder, Microsystem Technology 15 (2009) 401–406.
[8] R. Ibrahim, M.A. Omar, W.C. Goh, M. Mohamad, S. Muhamad, N.A. Yahya, Z. Radzi, N.H. Abu Kasim, Fabrication of 316L stainless steel parts by injection moulding for biomedical application using a novel binder, Biomedical 2006 IFME Proceedings 15 (2007) 102–105.
[9] M.A. Omar, I. Subuki., Rapid debinding of 316L stainless steel injection molded component using palm based biopolymer binder, in: Proceedings of the 3rd Colloquium on Materials, Minerals and Polymers, April 2007, (2007) 196–198.
[10] I. Subuki, M.A. Omar, M.H. Ismail, Z. Halim, Solvent extraction study of injection molded component using PS based binder, in: Proceedings of the 4th National Technical Postgraduate Symposium, May 2006.

[11] C. Quinard, T. Barriere, Development and properties identification of 316L stainless steel feedstock for PIM and μPIM, Powder Technology 190 (2008) 123–128.
[12] R.M. German, Workshop on scientific issues for medical and dental applications of micro/nano powder injection molding, sintering, modeling and commercial applications, Workshop on Medical and Dental Applications for MicroPIM (2009).
[13] R.M. German, A. Bose, Injection Molding of Metals and Ceramics, MPIF, Princeton, NJ, 1997.
[14] F.M. Foudzi, N. Muhamad, A.B. Sulong, H. Zakaria, Flow behaviour characteristic for injection process using nano-yttria stabilized zirconia for micro metal injection molding (μMIM), Applied Mechanics and Materials 44–47 (2011) 480–484.
[15] MPIF. Standard Test Methods for Metal Powders and Powder Metallurgy Products, Princeton, New Jersey, Metal Powder Industries Federation, 2006.
[16] R.M. German, Sintering Theory and Practise, John Wiley & Sons, Inc., 1996, p. 534.
[17] J.S. Lao, Z. Yi, B. Xiao, Y. Gao, Z.P. Xie, J.B. Li, Y. Huang, Injection molding of ultra-fine zirconia (Y-TZP) powders, Journal of Ceramic Processing Research 7 (2006) 14–19.
[18] J.K. Lee, Y.J. Kim, H. Kim, Formation of irregular grain shapes by ceria doping in 3 mol% yttria-stabilized zirconia ceramics, Materials Letters 33 (1998) 279–282.
[19] J.H. Song, J.R.G. Evans., The injection moulding of fine and ultra-fine zirconia powders, Ceramics International 21 (1995) 325–333.
[20] K.N. Hunt, J.R.G. Evans, J. Woodthorpe., The influence of mixing route on the properties of CIM blends, British Ceramic Transactions Journal 87 (1998) 17–21.
[21] Y. Li, L.J. Li, K.A. Khalil, Effect of powder loading on MIM stainless steel, Journal of Materials Processing Technology 183 (2007) 432–439.
[22] P.C. Yu, Q.F. Li, J.Y.H. Fuh, T. Li, L. Lu., Two-stage sintering of nano-sized yttria stabilized zirconia by powder injection molding, Journal of Material Processing Technology 192–193 (2007) 312–318.
[23] O. Reen, US Patent 4,032,336 (1997).
[24] L.-R. Christel, A. Florence, D. Celine, G. Manuel, R. Abel, Dense yttria stablized zirconia: sintering and microstructure, Ceramics International 29 (2003) 151–158.
[25] G. Antau, M. Ghislan, H. Francoise, C. Alain, C. Christian, Microstucture of partialliy stabilized zirconia manufactured via hyrid plasma spray process, Ceramics International 31 (2005) 611–619.